

3D elemental and structural analysis of biological specimens using electrons and ions

K. SCOTT

National Institute of Standards and Technology, Gaithersburg, Maryland, U.S.A.

Key words. Diatom, EDS, FIB, focused ion beam, SEM, X-ray microanalysis, 3D elemental mapping.

Summary

We demonstrate the utility of focused ion beam scanning electron microscopy combined with energy dispersive x-ray spectrometry for 3D morphological and elemental correlative analysis of subcellular features. Although recent advances in super-resolution light microscopy techniques and traditional transmission electron microscopy methods can provide cellular imaging at a wide range of length scales, simultaneous 3D morphological and elemental imaging of cellular features at nanometre scale can only be achieved with techniques such as focused ion beam scanning electron microscopy with energy dispersive x-ray spectrometry capability. We demonstrate the technique by analysing the 3D silicon cell wall structure of a marine diatom, *Thalassiosira pseudonana*. This study also highlights the limitations of the technique in its current state and suggests several possible improvements needed for the routine use of the technique for biological specimens.

Introduction

Biological specimens are inherently 3D objects and the investigation of these complex and interconnected structures can greatly benefit from 3D imaging at varying length scales. Although 3D imaging of biological surfaces based on stereoscopic techniques has been available since the early days of the scanning electron microscopes (Stewart & Snelling, 1965; Boyde & Williams, 1971; Dinnis, 1971; Catto & Smith, 1972; Boyde, 1974), traditionally, lower-resolution imaging of tissues and cells has been accomplished by light microscopy whereas high-resolution ultra-structural imaging has been carried out using scanning electron microscopy (SEM) or transmission electron microscopy (TEM). To date, 3D imaging of biological specimens has been largely limited to confocal light microscopy, although TEM tomographic techniques and single particle techniques are sometimes used for 3D

analysis of thin sections (50- to 100-nm-thick sections) or small particulate samples such as viruses or supramolecular complexes (Frank, 2006).

Recent advances in light microscopy techniques have enabled 3D imaging of cells at resolutions well below diffraction limits. (Shaevitz, 2008). Schmidt *et al.* (2008) demonstrated a 45 nm isotropic point spread function using a method based on stimulated emission depletion, whereas Juetten *et al.* reported $30 \times 30 \times 75$ nm resolution imaging in a thick sample (Juetten *et al.*, 2008; Schmidt *et al.*, 2008). However, many of these super-resolution techniques are based on fluorescence microscopy and cannot achieve comparable resolution for general ultra-structural investigation. On the other hand, SEM-based 3D imaging techniques such as focused ion beam (FIB) SEM and serial block-face SEM can be used to produce high-resolution 3D imaging of biological samples at 2 to 5 nm lateral resolution and 20 to 50 nm axial resolution (Denk & Horstmann, 2004; Heymann *et al.*, 2006; Giannuzzi *et al.*, 2007; Rouquette *et al.*, 2009; Schroeder-Reiter *et al.*, 2009; Zankel *et al.*, 2009).

When combined with 3D structural information, the spatial distribution patterns of chemical species or elements in the cellular environment can provide important insights into cellular processes and behaviour. Raman microscopy or fluorescence microscopy in conjunction with chemically specific tags are the commonly used techniques (Hell, 2003; Baker, 2010). However, these techniques have similar limitations as other light microscopy techniques. For example, Raman microscopy requires *a priori* knowledge of the chemical species in the sample whereas tag-based fluorescence microscopy cannot provide contextual information unless additional labels are used to delineate structural features. Until now optical microscopy techniques have been unable to routinely provide 3D chemical and morphological information at nanometre resolution. FIB SEM combined with energy dispersive x-ray spectrometry (EDS) can deliver 3D elemental maps and the corresponding 3D structural images (Kotula *et al.*, 2006; Schaffer *et al.*, 2007).

Although FIB SEM is a well established and widely used technique in the materials science fields and semiconductor

Correspondence to: K. Scott, National Institute of Standards and Technology, 100 Bureau Drive, MS-8372, Gaithersburg, MD 20899, U.S.A. Tel: 301 975 4579; fax: 301 417 1321; e-mail: keana.scott@nist.gov

industry, its use in biological imaging has been limited and the combined use of 3D FIB SEM and EDS imaging of biological specimens has not been reported previously. In this proof-of-concept study, we demonstrate the feasibility and the utility of the FIB SEM EDS technique for the 3D structural and elemental analysis of biological samples. Specifically, we present the 3D reconstruction of the silica shell of a diatom using the FIB SEM EDS method and discuss some of the key issues that arise when using FIB SEM EDS in the context of 3D biological analysis.

Diatoms are ubiquitous unicellular algae that are responsible for a large part of the oceanic primary production (Martin-Jézéquel *et al.*, 2000). They are roughly cylindrical in shape and about 4 μm in diameter and 7 μm in length. In addition to their role in biomass production, diatoms display an interesting biomineralization process of creating silicate nano-features (Frigeri *et al.*, 2006). In recent years, there has been much interest in learning how diatoms accomplish this biomineralization process. However, it is difficult to analyse the structural details of diatoms because the siliceous features shatter easily during the traditional sectioning processes. By applying the FIB SEM EDS technique to this problem, we demonstrate the utility of this technique for nano-characterization of biological materials such as diatoms.

Materials and methods

Sample preparation

The resin embedded sample of diatom species *Thalassiosira pseudonana* was supplied by Dr. Sriram Subramaniam (National Institutes of Health, Bethesda, MD, U.S.A.). Diatom culture was grown in artificial sea water medium (Darley & Volcani, 1969) supplemented with biotin and vitamin B12, each at 1 ng L^{-1} . Growth was at 18°C in continuous light at an intensity of 150 $\mu\text{mol m}^{-2} \text{s}^{-1}$. Aliquots of cells were fixed with equal volume of 0.2 M Na cacodylate, 5% glutaraldehyde in 3.5% NaCl for 15 min at room temperature (Hildebrand *et al.*, 2009). For plastic embedding, fixed cells were exposed to 1% aqueous osmium tetroxide for 1 h at room temperature, repeatedly rinsed with water, dehydrated using a graded ethanol–water mixtures followed by a final wash in acetone and embedded in epoxy resin (Heymann *et al.*, 2006). The resin block was trimmed to a pyramidal shape using a razor blade with a block face of about 2 mm^2 in area. The surface was smoothened by sectioning using a conventional 45° diamond knife from Diatome¹ (EMS, Hatfield, PA, U.S.A.). The entire pyramidal block was mounted on a scanning electron

microscope stub using silver paint (SPI Supplies, West Chester, PA, U.S.A.) such that the ultramicrotome-prepared block face was pointing up.

FIB milling, SEM imaging and x-ray spectrum imaging

FIB SEM EDS was performed on an FEI Nova 600 NanoLab (FEI, Hillsboro, OR, U.S.A.) equipped with an INCAx-sight Si(Li) EDS detector with 10 mm^2 active area, ultra-thin window, 35° take-off angle and 45° azimuthal angle with respect to the plane of the ion and electron columns (Oxford, Abingdon, Oxfordshire, U.K.). In an FIB scanning electron microscope, the ion beam and the electron beam are focused on the same region of the sample when the sample is at the coincidence height. Once the sample is at this coincidence height, the stage is tilted by 52° towards the ion column so that the sample surface is normal to the ion beam. A section of the sample is then removed or milled away using the FIB and the resulting face is imaged using the electron beam. An x-ray spectrum image of the same face can be acquired at this orientation as well (Goldstein *et al.*, 2003). Figure 1 illustrates the experimental geometry described here.

Prior to the FIB milling and SEM imaging, a 1- μm -thick layer of platinum is deposited over a region of interest as a protective layer. This platinum layer provides a smooth and robust (beam insensitive) surface that is effective in reducing milling artefacts such as curtaining (vertical grooves that are formed from uneven milling of the material) (Giannuzzi & Stevie, 2005). Once the protective layer is in place, several coarse cuts are made to create a U-shaped trench (dotted shape in Fig. 2) around the regions of interest (analysis volume). These trench cuts are made wide enough to allow a clear view of the exposed analysis face (represented by the XY face

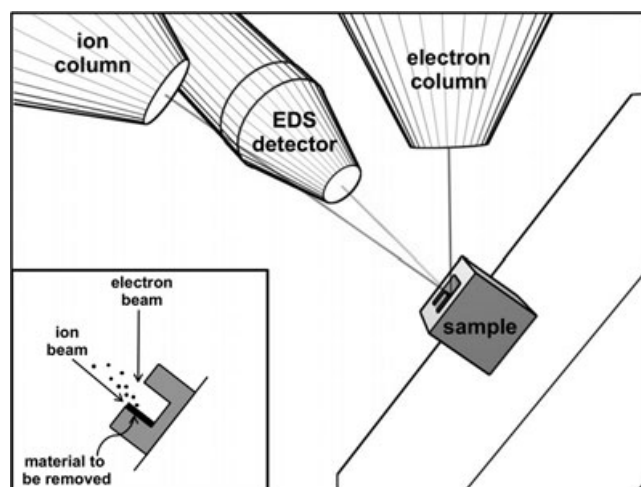


Fig. 1. Experimental geometry of the FIB SEM chamber showing the respective locations of the electron column, the ion column, the EDS detector and the sample. Inset is the schematic of material removal by ion beam.

¹Certain commercial equipment, instruments or materials are identified in this paper to foster understanding. Such identification does not imply recommendation or endorsement by the National Institute of Standards and Technology, nor does it imply that the materials or equipment identified are necessarily the best available for the purpose.

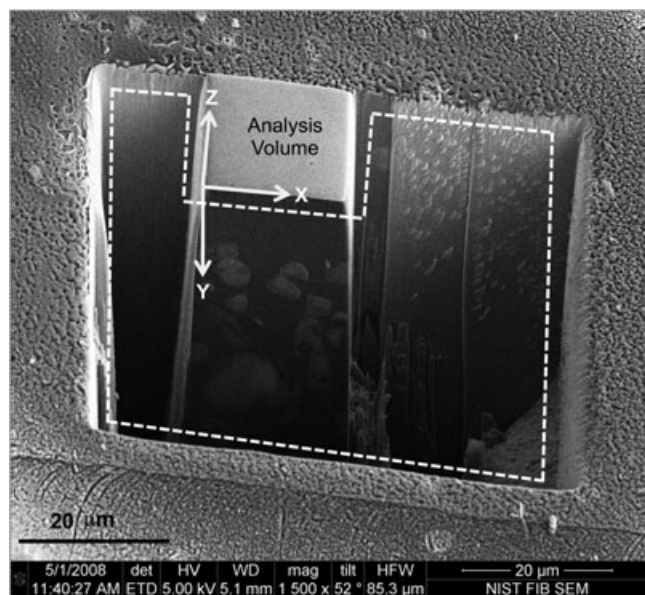


Fig. 2. Plastic embedded diatom sample prepared for serial milling and imaging process. The U-shaped trench (dotted shape) around the analysis volume allows the unobstructed imaging of the analysis face. XY-plane defines the analysis face and Z is the direction of material removal.

in Fig. 2) for SEM imaging as well as a clear line of sight path from the analysis face to the EDS detector (Schaffer *et al.*, 2007). All ion beam milling described in this work was performed at 30 kV ion beam accelerating voltage. However, different ion beam currents were used to achieve acceptable milling rate and surface finish. For example, most of the coarse cuts were made using 21 or 9.3 nA ion beam currents because we were more interested in removing large volumes of material rapidly than having a clean milled surface. Subsequent cleaning steps were performed at lower ion currents to ensure a smoother finish.

After the trench cuts were made, the resulting 30-μm-wide (X) and 50-μm-tall (Y) analysis face was cleaned using 2.8 nA ion beam current. SEM imaging and x-ray spectrum imaging were performed over a 10-μm-wide by 10-μm-tall region of the analysis face where the diatom concentration was relatively high. A layer of the sample (roughly 250 nm thick) was removed along the Z-direction and the SEM image and the x-ray spectrum image of the newly exposed face were collected. 3D SEM and x-ray spectrum image stacks were generated by repeating this process of serial milling and imaging. The processing and imaging time for each slice took about 40 min in all – 10 min for material removal, 1 min for SEM imaging, 20 min for X-ray imaging with 20% dead time and the time needed for mode switching and setup. Both the SEM image (2048 × 1988 pixels) and the spectrum image (256 × 224 pixels by 512 channels) were collected at 5 keV electron beam energy, 98 pA beam current. Each x-ray spectrum image was generated by summing about 40 frames of x-ray signal. A total

of 30 slices was processed in this manner consuming a roughly $30 \times 50 \times 7.5 \mu\text{m}$ region of the sample volume.

Several different approaches were initially tested in order to ensure consistent slice thickness. Regularly spaced tick marks were etched on a strip of platinum deposited near the region of interest and used as a guide in placing the milling patterns. However, degradation of these fiducial markers after repeated ion beam exposure limited the effectiveness of this approach. For the 3D analysis presented here, we used a distance between the milling pattern and a known feature on the sample surface to determine the next cut location.

Only two diatoms were represented/captured in their entirety within the analysis volume. The 3D reconstruction results presented here are derived from a diatom whose volume spanned 13 consecutive slices. SEM image segmentation, alignment and 3D volume generation were performed using IMAGEJ (Abramoff *et al.*, 2004) and AMIRA (Amira, 2008). In order to minimize the data file size, SEM images were cropped to contain regions surrounding the diatom of interest and resized to a larger format with zero padding to accommodate image shift during the alignment process. The cropped SEM images were manually segmented and aligned. A 3D volumetric mesh was generated using Amira's slice interpolation routine and tetrahedral volume generator function. For the 3D Si x-ray map, first the 2D background subtracted Si x-ray maps were extracted from the corresponding spectrum image stack using LISPIX (Bright, 2007) and custom MATLAB scripts (MATLAB, 2008). Once the Si maps were extracted, a volume reconstruction procedure similar to that used for the SEM images was used to create the final 3D rendering of the Si x-ray data.

Results and discussion

In this proof-of-concept experiment, we used FIB SEM EDS to analyse the 3D structural details and silicon distribution of a diatom. Figure 3 shows one of the Si x-ray maps and the corresponding SEM image. The box in Fig. 3B outlines the diatom selected for the 3D reconstruction results presented here. The SEM image is rotated ~30 degrees relative to the Si x-ray map. This rotation is due to a misalignment between the raster generated by the microscope and the raster generated by the EDS system for x-ray mapping. The resulting misregistration is easily corrected by rotating the final reconstructed volumes.

Diatoms such as *T. pseudonana* have silica-based cell wall structures with nano-scale patterns and are closely examined for their use in directed nanomaterial synthesis (Noll *et al.*, 2002; Vrieling *et al.*, 2005; Hildebrand *et al.*, 2006). One mechanism for silica nano- and micro-structure formation is the polymerization of silica from soluble precursors (Hildebrand *et al.*, 2009). However, exactly how these shapes are generated is not yet known. Accurate and improved detection of subcellular deposits of silica and identification

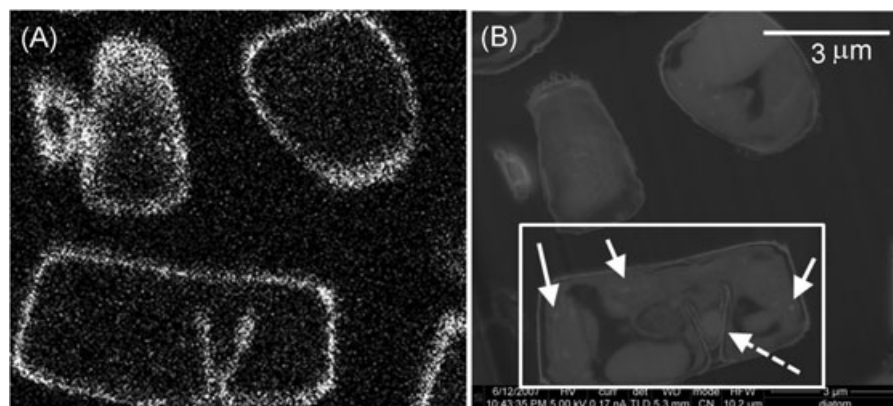


Fig. 3. A Si x-ray map (A) and the corresponding secondary electron image (B) from the serial milling and imaging data set. The diatom in the box in (B) was used for the 3D reconstruction. Solid arrows point to the bright punctate features in the diatom. Whether these features contain Si is of interest in determining diatom's bio-mineralization process. Dotted arrow shows a nascent cell wall that is being formed prior to cell division.

of distribution patterns can help further elucidate the biomineralization process in diatoms. When examining the SEM images of a diatom, one obvious question is whether the bright regions in the SEM image (indicated by the arrows in Fig. 3B) contain silicon. Because some of the subcellular organelles such as chloroplasts can produce similar contrast as silica structures, it is difficult to identify silica based on the SEM image alone. Although the silica cell wall and the nascent cell wall (indicated by the dotted arrow in Fig. 3B) are clearly visible, other similarly bright, punctate features did not show up in the corresponding Si x-ray map (Fig. 3A). Point analysis of these punctate features confirmed that they did not contain detectable amounts of silicon and they are mostly likely small lipid or starch deposits common in chloroplasts.

Figure 4 shows the 3D volumes generated from the SEM images (in green) and Si x-ray maps (in purple) of the diatom shown in Fig. 3. Although the overall shapes of both volumes are similar, some of the finer structural details are missing

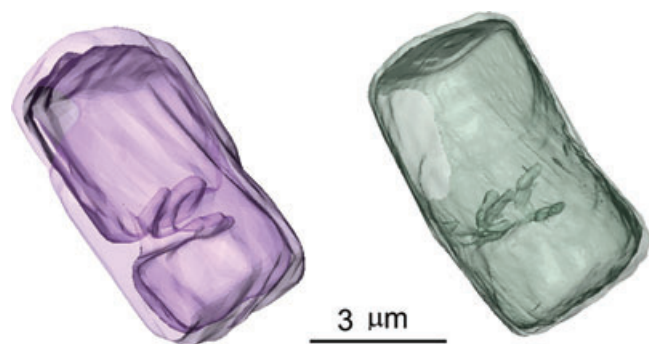


Fig. 4. 3D reconstruction of a diatom cell wall based on the Si x-ray maps (purple) and corresponding SEM images (green) using serial FIB milling and imaging. 3D volume generated from the x-ray maps does not show the finer structural details of the nascent cell wall because of the lower resolution of the x-ray maps compared to the SEM images.

in the Si x-ray volume. The low beam energy and low beam current conditions used in this experiment required a relatively long collection time (about 20 min clock time) per spectrum image in order to achieve a reasonable signal-to-noise level. Additionally, because the use of the drift correction algorithm increases the imaging time and decreases the field of view significantly, spectrum images were collected without any drift correction for this proof-of-concept study. As a result, noticeable image drift was present during the x-ray imaging and contributed to the significant loss of resolution.

Electron beam energy and the slice thickness used in this experiment were based on findings from an earlier study where the 3D elemental mapping artefacts in biological specimen were examined using Monte Carlo simulation of a diatom model (Scott & Ritchie, 2009). In that study, the authors concluded that electron beam energies greater than 5 keV would result in a beam-sample interaction volume too large to provide any useful structural information. The authors also concluded that the depth resolution of the x-ray maps collected using a 5 keV electron beam would be about 250 nm for biological specimens such as diatoms. Although for the Si analysis presented here, electron beam energy of 3 keV rather than 5 keV would have been more effective and less damaging to the sample, 5 keV electron beam energy was used to assess the feasibility of FIB SEM EDS analysis for studying the fate of nanoparticles such as quantum dots in biological specimens.

In addition to the Monte Carlo simulations of a model system, several additional x-ray spectrum imaging conditions such as dwell time and beam current were experimentally tested for optimal SEM and x-ray spectrum imaging results. After trying various dwell time and beam current combinations, 100 µs pixel dwell time at 5 keV beam energy with 98 pA electron beam current were selected for the final experiment. For the diatom sample used in this study, beam energies greater than 5 keV and/or beam current higher than 98 pA resulted in noticeable sample damage and poor depth (Z)

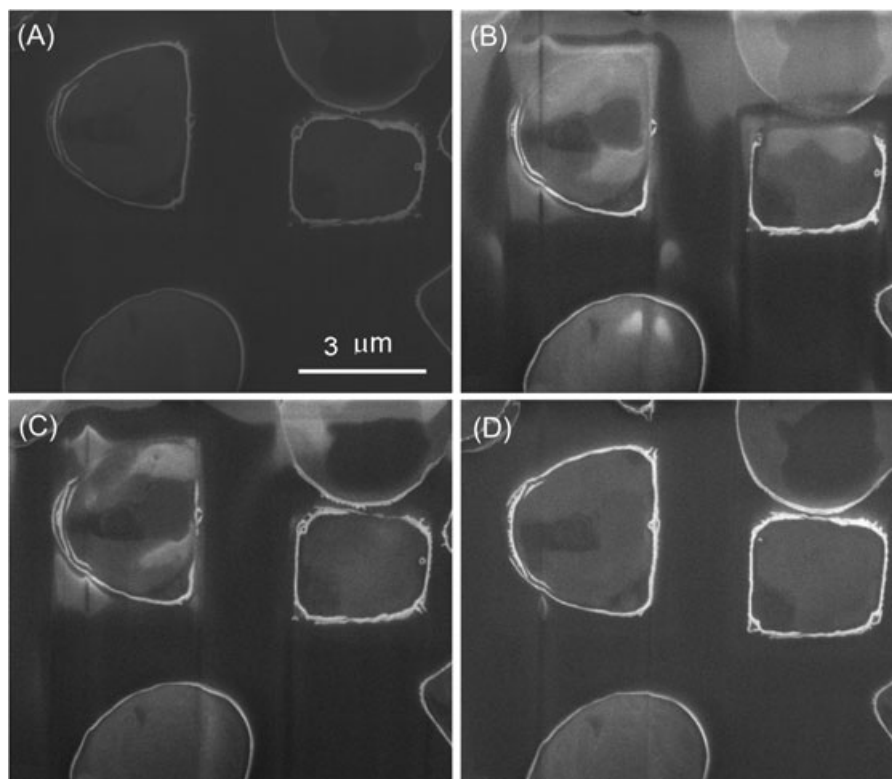


Fig. 5. Beam induced sample damage from a 15 min spectrum imaging run using 5 keV, 0.17 nA electron beam conditions. Panels represent the sample faces (A) before the x-ray spectrum imaging was performed and after removing (B) 300 nm, (C) 500 nm and (D) 800 nm layers from the original analysis face.

resolution. Figure 5 shows the SEM images of the analysis face before and after a spectrum imaging run. For this particular case, a spectrum image was collected over 15 min (clock time) using 5 keV beam energy and 0.17 nA beam current. Figure 5(A) is the clean undamaged sample face prior to x-ray spectrum imaging. After the spectrum image was collected, a 100-nm-thick layer was removed from the analysis face and the SEM image of the newly exposed face was collected and this process was repeated several times until there was no detectable beam damage in the sample. Figure 5(B)–(D) are the third, fifth and the eighth of this series of images corresponding to the post-analysis sample condition 300, 500 and 800 nm below the original analysis face, respectively. As shown in Fig. 5(C), even after a 500-nm-thick layer of the sample was removed, the effects of the beam induced sample damage are significant enough to obscure major structural features of the diatoms. The integrity of the sample face is not restored until an 800-nm-thick layer of the sample is removed (Fig. 5D). Therefore the depth resolution, at this high beam current condition, is effectively reduced to about 800 nm because smaller section steps will result in unusable images.

Another important factor in FIB-SEM-based EDS analysis is the size of the unobstructed space around the analysis volume. Insufficiently sized coarse trench cuts around the block face

have a large effect on the quality of the SEM images and the x-ray maps (Giannuzzi & Stevie, 2005; Kotula *et al.*, 2006). Figure 6 illustrates this problem. In Fig. 6(A), the trench cut below the analysis volume is too narrow and only part of the FIB milled face can be imaged and analysed. A narrow trench cut will result in uneven contrast as well as obstructions due to re-deposition of milled material around the sample analysis face. Similarly, the amount of free space on the side closer to the EDS detector can affect the efficiency of x-ray signal detection. Figure 6(B) shows the sample geometry and relative position of the EDS detector in our experimental setup. It is obvious that a sufficiently wide trench is needed on the right side of the analysis volume to ensure a clear line-of-sight path from the entire analysis face to the EDS detector. This problem is clearly illustrated in Fig. 7. Figure 7(A) is the SEM image of the entire block face and surrounding trenches. The box on the right side of the block face indicates the area where spectrum imaging was performed and the arrow indicates the direction of the EDS detector. The box in Fig. 7(B) shows the area where the x-ray spectrum image was collected from and Fig. 7(C) and (D) are the corresponding oxygen and silicon maps. In this example, the trench on the side of the EDS detector (right side) is too narrow and the oxygen and silicon x-ray signals from the right half of the analysis face are blocked by the side wall of the trench. To minimize the shadowing and spurious x-ray signals

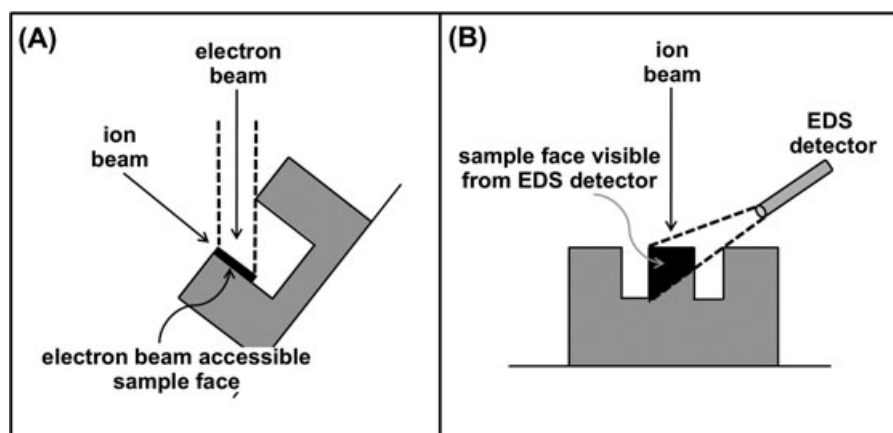


Fig. 6. Cut-away view of the sample exposing the analysis face and the surrounding trench in relation to (A) the electron and the ion beams and (B) the EDS detector. The size of the bottom trench determines the amount of sample face available for SEM imaging (A) and the size of the right trench affects the emitted x-ray detection efficiency.

from material surrounding the analysis volume, Schaffer *et al.* (2008) recently proposed a block lift-out method, where the analysis volume is lifted out of the bulk material and analysed while suspended from a micromanipulator probe tip. Placing the lift-out volume on a low-background substrate can provide

similar advantage with added sample manoeuvrability (Scott *et al.*, 2009).

It is widely accepted that low beam energy (5 keV or less) x-ray analysis is fraught with additional complications compared to traditional x-ray analysis (Echlin, 2001). For

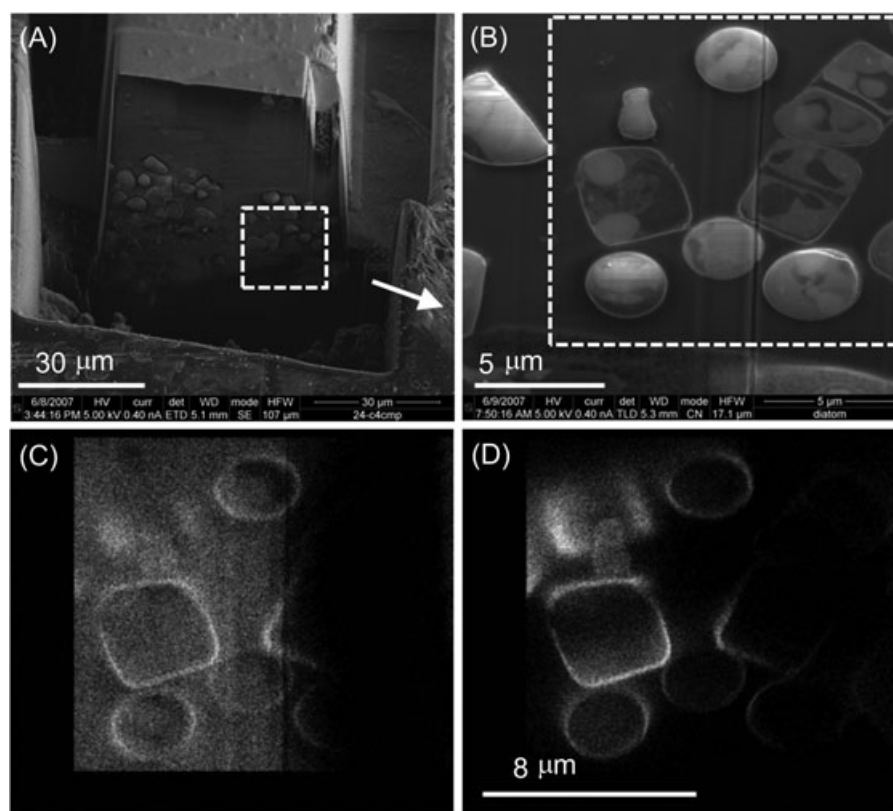


Fig. 7. Effects of low EDS detector takeoff angle and insufficient line-of-sight clearance. (A) An overview image of the volume of interest with a narrow trench cut. Dotted box indicate the area where x-ray analysis was performed and the arrow indicates the direction of the EDS detector. (B) A close-up image of the analysis face and (C) oxygen and (D) silicon x-ray maps from the dotted box area.

example, at 5 keV the signal-to-noise ratio is quite poor and relatively long acquisition times are required to collect statistically significant x-ray maps. And, as mentioned earlier, long x-ray imaging time increases the likelihood of image and sample drift and thus loss of overall resolution. To generate the 3D SEM and x-ray volumes presented here, over 15 h of milling and imaging was required in addition to the sample preparation time such as finding the volume of interest or making the trenches around the volume of interest. For future experiments, the use of a silicon drift detector with a larger solid angle in place of the Si(Li) detector used in this experiment might improve the spectrum imaging efficiency.

Not only is the time required for milling and imaging a biologically relevant sample volume (say $40 \times 40 \times 40 \mu\text{m}$ to capture a small cell in its entirety) prohibitive to apply the FIB SEM EDS technique for routine analyses, there is an additional bottleneck. The difficulty of finding an appropriate volume of interest is surprisingly high. For 3D FIB SEM EDS analysis, cells or tissues are embedded in plastic and trimmed to expose the area of the plastic with high concentration of cells. However, finding the relevant cell or the area of tissue becomes extremely time consuming because of the electron opaque nature of the plastic sample and the sparse distribution of the sample material. For example, let us consider cells with nominal diameter of $10 \mu\text{m}$ embedded in plastic. Even if the cells are pre-concentrated into a pellet, they tend to spread apart during the embedding process. That means in a given FIB SEM EDS analysis volume, there will be only a handful of cells and capturing a cell or a feature of interest in its entirety can be difficult. For effective FIB SEM EDS analyses of biological samples, pre-concentration of the biological material and proper trimming of the sample block are prerequisites.

Conclusions

In this study, the feasibility and the utility of a novel 3D x-ray mapping technique for biological specimen was evaluated. Although 3D x-ray mapping of biological specimen is possible and can provide additional insights for understanding of key physiological processes not accessible from high-resolution morphological data alone, the technique is in its infancy and there are several important factors that should be considered. In our study, the combination of the low electron beam energy and the small detector takeoff angle created considerable challenges for effective spectrum imaging. The usual trick of increasing the beam current to increase the x-ray production could not be used due to the beam sensitivity of the sample. This limitation is true for most biological samples. Additionally, the long data acquisition time required in the current setup makes 3D elemental analysis of a large feature such as an entire cell ($>20 \mu\text{m}$ in diameter in many cases) all but impossible as a routine procedure although the analysis of small ($<5 \mu\text{m}$) subcellular regions can be done more easily. To enable routine use of the FIB SEM EDS technique for biological specimens,

several major challenges need to be addressed: (1) an effective sample surveying and preparation methods such as *in situ* x-ray tomography and large volume milling capabilities; (2) a faster and more sensitive x-ray imaging solutions such as multi-detector configuration and large area silicon drift detectors and (3) high-resolution imaging at biologically relevant length scale via the use of high-density detectors or efficient stitching algorithms. However, some of the newer FIB SEM systems now provide the large area imaging as well as automated 3D analysis capabilities, making FIB-SEM-based x-ray microanalysis more accessible for routine biological studies.

Acknowledgement

Dr. Sriram Subramaniam from the National Cancer Institute is gratefully acknowledged for supplying the diatom sample.

References

- Abramoff, M.D., Magelhaes, P.J. & Ram, S.J. (2004) Image processing with ImageJ. *J. Biophoton. Int.* **11**, 36–42.
- Amira. (2008) <http://www.amira.com/index.html>. Visage Imaging, Carlsbad, CA. Last accessed: 04/06/2010.
- Baker, M. (2010) Laser tricks without labels. *Nat. Methods* **7**, 261–265.
- Boyde, A. (1974) Three-dimensional aspects of SEM images. *Scanning Electron Microscopy* (ed. by O.C. Wells), pp. 277–307. McGraw-Hill, New York.
- Boyde, A. & Williams, R.A.D. (1971) Estimation of the volumes of bacterial cells by scanning electron microscopy. *Arch. Oral Biol.* **16**, 259–267.
- Bright, D. (2007) *Lispix*, <http://www.nist.gov/lispix/doc/contents.htm>. Last accessed: 04/06/2010.
- Catto, C.J.D. & Smith, K.C.A. (1972) A storage-display system for the scanning electron microscope. *Proc. 5th Annual Scanning Electron Microscopy Symposium*, pp. 41–48, Chicago, IL.
- Darley, W.M. & Volcani, B.E. (1969) Role of silicon in diatom metabolism: a silicon requirement for deoxyribonucleic acid synthesis in the diatom *Cylindrotheca Fusiformis* Reimann and Lewin. *Exp. Cell Res.* **58**, 334–342.
- Denk, W. & Horstmann, H. (2004) Serial block-face scanning electron microscopy to reconstruct three-dimensional tissue nanostructure. *PLoS Biol.* **2**, 1900–1909.
- Dinnis, A.R. (1971) After-lens deflection and its uses. *Proc. 4th Annual Scanning Electron Microscopy Symposium*, pp. 41–48, Chicago, IL.
- Echlin, P. (2001) Biological x-ray microanalysis: the past, present practices, and future prospects. *Microsc. Microanal.* **7**, 211–219.
- Frank, J. (2006) *Electron Tomography*, 2nd edn. Springer, New York.
- Frigeri, L.G., Radabaugh, T.R., Haynes, P.A. & Hildebrand, M. (2006) Identification of proteins from a cell wall fraction of the diatom *Thalassiosira pseudonana*: insights into silica structure formation. *Mol. Cell. Proteomics* **5**, 182–193.
- Giannuzzi, L.A. & Stevie, F.A. (2005) *Introduction to Focused Ion Beams*. Springer, New York.
- Giannuzzi, L.A., Phifer, D., Giannuzzi, N.J. & Capuano, M.J. (2007) Two-dimensional and 3-dimensional analysis of bone/dental implant interfaces with the use of focused ion beam and electron microscopy. *J. Oral. Maxillofac. Surg.* **65**, 737–747.

- Goldstein, J., Newbury, D., Joy, D. *et al.* (2003) *Scanning Electron Microscopy and X-Ray Microanalysis*, 3rd edn., pp. 496–497. Springer, New York.
- Hell, S. (2003) Toward fluorescence nanoscopy. *Nat. Biotech.* **21**, 1347–1355.
- Heymann, J.A.W., Hayles, M., Gestmann, I., Giannuzzi, L.A., Lich, B. & Subramaniam, S. (2006) Site-specific 3D imaging of cells and tissues with a dual beam microscope. *J. Struct. Biol.* **155**, 63–73.
- Hildebrand, M., York, E., Kelz, J.L., Davis, A.K., Frigeri, L.G., Allison, D.P. & Doktycz, M.J. (2006) Nano-scale control of silica morphology and three-dimensional structure during diatom cell wall formation. *J. Mater. Res.* **21**, 2689–2698.
- Hildebrand, M., Kim, S., Shi, D., Scott, K. & Subramaniam, S. (2009) 3D imaging of diatoms with ion abrasion scanning electron microscopy. *J. Struct. Biol.* **166**, 316–328.
- Juette, M.F., Gould, T.J., Lessard, M.D. *et al.* (2008) Three-dimensional sub-100 nm resolution fluorescence microscopy of thick samples. *Nat. Methods* **5**, 527–529.
- Kotula, P.G., Keenan, M.R. & Michael, J.R. (2006) Tomographic spectral imaging with multivariate statistical analysis: comprehensive 3D microanalysis. *Microsc. Microanal.* **12**, 36–48.
- Martin-Jézéquel, V., Hildebrand, M. & Brzezinski, M. (2000) Silicon metabolism in diatoms: implications for growth. *J. Phycol.* **36**, 821–840.
- MATLAB. (2008) <http://www.mathworks.com/products/matlab>. The MathWorks, Natick, MA, USA. Last accessed: 04/06/2010.
- Noll, F., Sumper, M. & Hampp, N. (2002) Nanostructure of diatom silica surfaces and of biomimetic analogues. *Nano Lett.* **2**, 91–95.
- Rouquette, J., Genoud, C., Vazquez-Nin, G.H., Kraus, B., Cremer, T. & Fakan, S. (2009) Revealing the high-resolution three-dimensional network of chromatin and interchromatin space: a novel electron-microscopic approach to reconstructing nuclear architecture. *Chromosome Res.* **17**, 801–810.
- Schaffer, M., Wagner, J., Schaffer, B., Schmied, M. & Mulders, H. (2007) Automated three-dimensional X-ray analysis using a dual-beam FIB. *J. Ultramicrosc.* **107**, 587–597.
- Schaffer, M., Schröttner, H. & Wagner, J. (2008) 3D Energy-dispersive x-ray spectrometry (3D EDXS) in a dualbeam FIB: aspects of sample preparation and quantitative analysis. *Microsc. Microanal.* **14**(Supp 2), 982–983.
- Schmidt, R., Wurm, C.A., Jakobs, S., Engelhardt, J., Egner, A. & Hell, S.W. (2008) Spherical nanosized focal spot unravels the interior of cells. *Nat. Methods* **5**, 539–544.
- Schroeder-Reiter, E., Perez-Willard, F., Zeile, U. & Wanner, G. (2009) Focused ion beam (FIB) combined with high resolution scanning electron microscopy: A promising tool for 3D analysis of chromosome architecture. *J. Struct. Biol.* **165**, 97–106.
- Scott, K. & Ritchie, N.W.M. (2009) Analysis of 3D elemental mapping artefacts in biological specimens. *J. Microsc.* **233**, 331–339.
- Scott, K., Davis, J.M. & Vicenzi, E.P. (2009) Three-dimensional microranalysis using FIB SEM: variations in technique. *Microsc. Microanal.* **15**(Supp 2), 476–477.
- Shaevitz, J.W. (2008) Super-resolution for a 3D world. *Nat. Methods* **5**, 471–472.
- Stewart, A.D.G. & Snelling, M.A. (1965) A new scanning electron microscope. *Proc. 3rd European Conf. Electron Microsc.*, pp. 55–56. Prague.
- Vrieling, E.G., Sun, Q., Beelen, T.P., Hazelaar, S., Gieskes, W.W., van Santen, R.A. & Sommerdijk, N.A. (2005) Controlled silica synthesis inspired by diatom silicon biomineralization. *J. Nanosci Nanotechnol.* **5**, 68–78.
- Zankel, A., Kraus, B., Poelt, P., Schaffer, M. & Ingolic, E. (2009) Ultramicrotomy in the ESEM, a versatile method for materials and life sciences. *J. Microsc.* **233**, 140–148.